



# Electrolyte Solvation Manipulation Enables Unprecedented Room-Temperature Calcium-Metal Batteries

Yulin Jie<sup>+</sup>, Yunshu Tan<sup>+</sup>, Linmei Li<sup>+</sup>, Yehu Han, Shutao Xu, Zhenchao Zhao, Ruiguo Cao,<sup>\*</sup> Xiaodi Ren, Fanyang Huang, Zhanwu Lei, Guohua Tao,<sup>\*</sup> Genqiang Zhang, and Shuhong Jiao<sup>\*</sup>

**Abstract:** Calcium-metal batteries (CMBs) provide a promising option for high-energy and cost-effective energy-storage technology beyond the current state-of-the-art lithium-ion batteries. Nevertheless, the development of room-temperature CMBs is significantly impeded by the poor reversibility and short lifespan of the calcium-metal anode. A solvation manipulation strategy is reported to improve the plating/stripping reversibility of calcium-metal anodes by enhancing the desolvation kinetics of calcium ions in the electrolyte. The introduction of lithium salt changes the electrolyte structure considerably by reducing coordination number of calcium ions in the first solvation shell. As a result, an unprecedented Coulombic efficiency of up to 99.1% is achieved for galvanostatic plating/stripping of the calcium-metal anode, accompanied by a very stable long-term cycling performance over 200 cycles at room temperature. This work may open up new opportunities for development of practical CMBs.

**M**ultivalent secondary batteries (Mg, Ca, Zn, Al, and so on) have received increased attention because of their potential as post Li-ion battery technology to meet the growing demand for future energy-storage applications.<sup>[1]</sup> Among them, Ca

batteries are strongly positioned because of the abundance and low cost of Ca, together with a two-electron redox chemistry leading to high energy density.<sup>[2]</sup> The abundance of Ca in the Earth's crust is approximately 4.15 wt%, which is the fifth most abundant element, and certainly less rare than elemental Li with an abundance of 0.002 wt%. Moreover, as an ideal choice for metallic anodes, Ca metal has a very low reduction potential of  $-2.87$  V versus a standard hydrogen electrode (SHE), which is very close to that of Li metal ( $-3.04$  V vs. SHE) and much lower than Mg ( $-2.37$  V vs. SHE), Al ( $-1.68$  V vs. SHE), and Zn ( $-0.76$  V vs. SHE).<sup>[3]</sup> Although Ca-metal anodes offer a lower gravimetric capacity compared with Li-metal anodes, they can deliver a higher volumetric capacity (ca.  $2073$  mAh cm<sup>-3</sup>). The combination of a low reduction potential and two-electron redox chemistry infers that, in principle, Ca-metal batteries (CMBs) could offer high energy density compared to state-of-the-art Li-ion batteries. Compared to its divalent counterpart, Mg-metal batteries, CMBs have a broader choice of cathode materials and deliver a better rate capability because of the lower charge density of Ca<sup>2+</sup>, thereby leading to faster solid-state diffusion in cathode materials.<sup>[4]</sup>

Although CMBs hold great promise for achieving high energy densities, grand challenges need to be overcome before practical CMBs may be developed; in particular, a lack of suitable electrolytes for reversible Ca-metal plating/stripping at room temperature.<sup>[5]</sup> Pioneering studies reveal that the reversibility of Ca-metal anodes is very poor in many commonly used nonaqueous electrolytes containing organic solvents, such as SOCl<sub>2</sub>, acetonitrile (ACN),  $\gamma$ -butyrolactone (GBL), propylene carbonate (PC), and tetrahydrofuran (THF), because passivation layers are formed.<sup>[5a]</sup> These passivation layers on the electrode surface typically contain species such as CaCl<sub>2</sub>, CaF<sub>2</sub>, CaO, CaCO<sub>3</sub>, and Ca(OH)<sub>2</sub>—most of which have good stability thermodynamically and low ionic conductivity. Although Ca stripping can be achieved at very high overpotential in some organic electrolytes, poor ionic conductivity drastically blocks the transport of Ca ions through the passivation layers and renders the plating of Ca metal impossible in traditional electrolytes.<sup>[5a]</sup> Therefore, Ca is significantly different from its Mg counterpart, which can be cycled reversibly in a variety of nonaqueous electrolytes.<sup>[1e,3b,6]</sup>

Although the overwhelming challenges facing Ca-metal anodes seem insurmountable, recent research has rekindled hope for development of practical CMBs. Ponrouch and co-workers reported that Ca plating was realized in a conventional organic electrolyte containing Ca(BF<sub>4</sub>)<sub>2</sub> as a Ca salt and a mixture of ethylene carbonate (EC) and PC as solvents.<sup>[7]</sup> Notably, the reversible plating/stripping of Ca metal can be

[\*] Y. Jie,<sup>[†]</sup> Y. Han, Prof. R. Cao, Prof. X. Ren, F. Huang, Z. Lei, Prof. G. Zhang, Dr. S. Jiao  
Hefei National Laboratory for Physical Science at the Microscale  
CAS Key Laboratory of Materials for Energy Conversion  
University of Science and Technology of China  
Hefei 230026 (P. R. China)  
E-mail: rgcao@ustc.edu.cn  
jiaosh@ustc.edu.cn

Y. Tan,<sup>[†]</sup> Prof. G. Tao  
School of Advanced Materials  
Shenzhen Key Laboratory of New Energy Materials by Design  
Peking University Shenzhen Graduate School  
Shenzhen 518055 (P. R. China)  
E-mail: taogh@pkusz.edu.cn  
Dr. L. Li<sup>[†]</sup>  
Department of biotechnology, Dalian Institute of Chemical Physics  
Chinese Academy of Sciences  
Dalian 116023 (P. R. China)  
Prof. S. Xu, Dr. Z. Zhao  
National Engineering Laboratory for Methanol to Olefins, Dalian  
National Laboratory for Clean Energy, iChEM, State Key Laboratory of Catalysis, Dalian Institute of Chemical Physics  
Chinese Academy of Sciences  
Dalian 116023 (P. R. China)

[†] These authors contributed equally to this work.

 Supporting information and the ORCID identification number(s) for the author(s) of this article can be found under:  
 <https://doi.org/10.1002/anie.202002274>.

only achieved at elevated temperature (75–100 °C) under small capacity cycling conditions (0.165 mAh cm<sup>-2</sup>). A large amount of CaF<sub>2</sub> was observed in the deposit, which was most likely part of the surface passivation layer. Despite the low efficiency and short cycling life, these results suggested the feasibility of a reversible Ca-metal anode for the first time. Recently, the first room-temperature Ca plating/stripping was realized in an electrolyte of 1.5 M Ca(BH<sub>4</sub>)<sub>2</sub> in THF, achieving a relatively high Coulombic efficiency (CE) of 94–96% with a short lifespan of up to only 50 cycles.<sup>[4]</sup> In this electrolyte system, the dominant deposit was Ca metal, together with a small fraction of CaH<sub>2</sub> distributed throughout the whole deposited film. More recently, room-temperature Ca plating/stripping was achieved by a new fluorinated alkoxy borate salt, Ca(B(OHfp)<sub>4</sub>)<sub>2</sub> (hfp = CH(CF<sub>3</sub>)<sub>2</sub>), dissolved in 1,2-dimethoxyethane (DME).<sup>[8]</sup> Another strategy for improving the reversibility of the Ca-metal anode is through formation of alloy compounds with Sn or using intercalation structure such as carbon.<sup>[9]</sup> Despite the aforementioned preliminary attempts to build a proof of concept for a reversible Ca-metal anode, this technology remains far from the realization of a practical CMB prototype. Most previous works are conducted with a three-electrode cell configuration and the Ca-anode performance needs to be improved significantly in terms of CE and cycling life. Moreover, the puzzling mechanisms behind Ca plating/stripping remain elusive.

Electrolyte solvation structure plays essential roles in all battery systems. The solvation energy is closely related to interfacial reactions on the electrode surface and eventually dictates the battery performance. Manipulation of electrolyte solvation structure is an effective way in which to improve the reversibility of metallic anodes such as Li, Na, and Mg.<sup>[10]</sup> Herein, we report a facile yet novel approach to significantly improve the reversibility of Ca-metal anodes by simply manipulating the solvation structure in an electrolyte containing 0.4 M Ca(BH<sub>4</sub>)<sub>2</sub> and 0.4 M LiBH<sub>4</sub> in THF (Ca(BH<sub>4</sub>)<sub>2</sub>-LiBH<sub>4</sub>-THF). Nuclear magnetic resonance (NMR) spectroscopy and theoretical calculations results reveal that the presence of Li<sup>+</sup> dramatically decreases the coordination number of Ca<sup>2+</sup> in the first solvation shell, thus weakening the solvation energy of Ca<sup>2+</sup> in the Ca(BH<sub>4</sub>)<sub>2</sub>-LiBH<sub>4</sub>-THF electrolyte. With such pronounced differences in the solvation structure, room-temperature plating and stripping of the Ca-metal anode is achieved with a spherical deposited morphology that is golf-ball-like in shape. With a coin-type cell configuration, an unprecedentedly high CE is achieved up to 99.1% with an ultralong lifespan over 200 cycles. The electrolyte of (Ca(BH<sub>4</sub>)<sub>2</sub>-LiBH<sub>4</sub>-THF) was prepared by directly dissolving Ca(BH<sub>4</sub>)<sub>2</sub> and LiBH<sub>4</sub> into THF. The electrolyte was stirred overnight to ensure dissolution of the solutes. The concentration of Ca(BH<sub>4</sub>)<sub>2</sub> and LiBH<sub>4</sub> was examined by inductively coupled plasma mass spectrometry (ICP-MS).

The feasibility of reversible Ca plating in the Ca(BH<sub>4</sub>)<sub>2</sub>-LiBH<sub>4</sub>-THF electrolyte was evaluated using the CE of the galvanostatic plating/stripping

processes on the Au electrode. The CE of the Ca-metal anode was measured by the ratio of galvanostatic stripping capacity to plating capacity in Ca||Au coin-type cells at room temperature. As shown in Figure 1a, highly reversible Ca-metal plating/stripping can be achieved in the Ca(BH<sub>4</sub>)<sub>2</sub>-LiBH<sub>4</sub>-THF electrolyte. The CE for the first plating/stripping cycle reaches 84.4% and increases up to 99.1% after only 5 cycles. Remarkably, an unprecedented average CE of 97.6% is obtained over 200 plating/stripping cycles. This performance outperforms all of the reported electrolytes in the literature in terms of the average CE and cycling life (Supporting Information, Figure S1). Notably, Ca plating/stripping on a Cu electrode also shows good reversibility with a comparably lower CE and shorter lifespan, indicating that substrate has impact on cycling performance. In contrast, the electrolyte of 1.5 M Ca(BH<sub>4</sub>)<sub>2</sub> in THF (Ca(BH<sub>4</sub>)<sub>2</sub>-THF) demonstrates very poor cycling stability on both Au and Cu electrodes. The CE of the Ca-metal anode exhibits severe fluctuation around 80% for the first 10 cycles, followed by a gradual decay down to 60% after 20 cycles. The Ca(BH<sub>4</sub>)<sub>2</sub>-THF electrolyte was further checked in a three-electrode cell configuration and the CE reached 94% (Figure S2), which is in good agreement with the previous report.<sup>[4]</sup> Figure 1c and Figure S3 show the corresponding voltage–capacity profile for the galvanostatic Ca-metal plating/stripping processes in the Ca(BH<sub>4</sub>)<sub>2</sub>-LiBH<sub>4</sub>-THF electrolyte. The overpotential for the first plating process was around 200 mV with a nucleation overpotential at about 323 mV versus Ca/Ca<sup>2+</sup>. The first stripping process can be realized by a very low overpotential at about 130 mV versus Ca/Ca<sup>2+</sup>. The overpotentials for plating and stripping decrease gradually down to about 97 mV versus Ca/Ca<sup>2+</sup> after 5 cycles, along with an increase of CE up to 99.1%. The Ca||Au cells undergo 200 discharge/charge

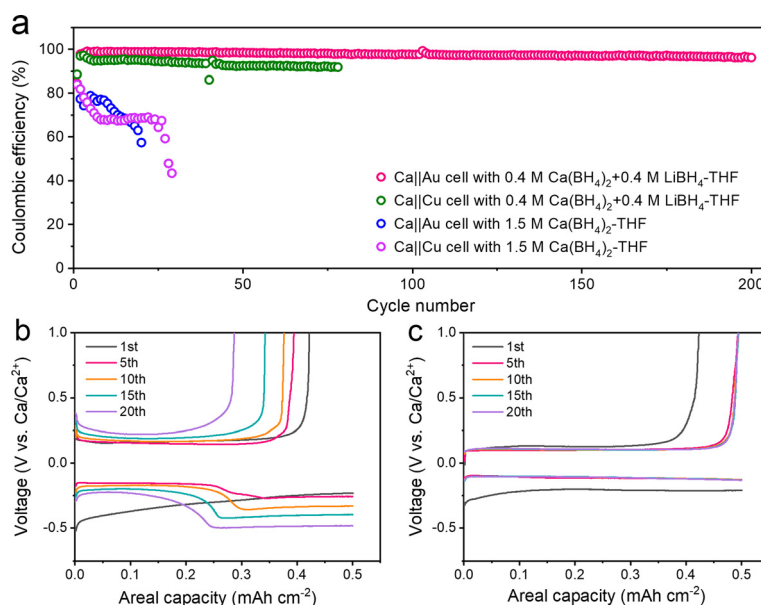


**Figure 1.** a) CE values of Ca||Au and Ca||Cu coin cells using Ca(BH<sub>4</sub>)<sub>2</sub>-LiBH<sub>4</sub>-THF and Ca(BH<sub>4</sub>)<sub>2</sub>-THF electrolytes at 1 mA cm<sup>-2</sup> and 0.5 mAh cm<sup>-2</sup>. Voltage–capacity profile of selected cycles on Au electrodes in b) the Ca(BH<sub>4</sub>)<sub>2</sub>-THF electrolyte and c) the Ca(BH<sub>4</sub>)<sub>2</sub>-LiBH<sub>4</sub>-THF electrolyte.

cycles with low overpotentials and high CEs, which suggests a stable and kinetically favored Ca-metal plating/stripping behavior. On the other hand, the overpotentials for Ca plating and stripping in the  $\text{Ca}(\text{BH}_4)_2$ -THF electrolyte are much higher than that in the  $\text{Ca}(\text{BH}_4)_2$ -LiBH<sub>4</sub>-THF electrolyte. As shown in Figure 1b, the nucleation overpotential for the first plating process is about 500 mV versus  $\text{Ca}/\text{Ca}^{2+}$ , along with a growth overpotential ranging from 500–400 mV versus  $\text{Ca}/\text{Ca}^{2+}$  (Figure S3). The improved electrochemical kinetics of the Ca-metal anode in  $\text{Ca}(\text{BH}_4)_2$ -LiBH<sub>4</sub>-THF are also reflected by the cyclic voltammetry (CV) test in a coin-type cell. The onset potential for Ca plating is much more positive in  $\text{Ca}(\text{BH}_4)_2$ -LiBH<sub>4</sub>-THF than in the  $\text{Ca}(\text{BH}_4)_2$ -THF electrolyte (Figure S4).

The speciation of galvanostatic plating was thoroughly explored by various characterization techniques, including X-ray diffraction (XRD), ICP-MS, X-ray photoelectron spectroscopy (XPS), and energy-dispersive X-ray spectroscopy (EDX). The XRD pattern of deposits present sharp peaks centered at approximately 27.6, 45.8, and 54.3° (Figure S5), corresponding to (111), (220), and (311) planes for the cubic  $Fm\bar{3}m$  crystalline phase of Ca (Ca-PDF No. 23-0430), which provides direct evidence of the generation of metallic Ca. Since the redox potential of Ca is close to Li (0.17 V vs.  $\text{Li}/\text{Li}^+$ ), the possibility of Li plating is prevented. Table S1 presents a ICP-MS speciation analysis of deposits derived from the first plating process, revealing a large fraction of Ca and a small amount of Li. The small amount of Li (ca. 2.4% of the plating capacity) may come from the surface-adsorbed species and formation of a LiAu alloy.

The morphology of deposits on Au electrodes in the  $\text{Ca}(\text{BH}_4)_2$ -LiBH<sub>4</sub>-THF electrolyte was studied by scanning electron microscopy (SEM). Figures 2a and 2b are representative of the morphology of the deposits; that is, spherical particles scattered on a gold thin film evaporated on a Cu electrode. The Ca particle has a microsized spherical shape with a golf-ball-like dimpled surface. The advantage of the spherical morphology is a reduced possibility to penetrate through the separator and cause a short-circuit hazard. The EDX mapping results suggest that the deposited particles are Ca with a small amount of carbon and oxygen on the surface (Figure 2c). The Ca deposits formed in the  $\text{Ca}(\text{BH}_4)_2$ -THF electrolyte severely penetrate into the separator and are very difficult to extract (Figure S6). The poor adhesion of the plated Ca indicates that it easily loses contact with the electrode, which may account for the bad cycling performance. To investigate the composition of the passivation layer and further confirm Ca-metal plating/stripping, the deposits formed in  $\text{Ca}||\text{Au}$  coin cells were examined by XPS (Figure 2d; Figure S7). XPS depth profiling analysis of deposits clearly shows the existence of metallic Ca after ion sputtering, without presenting distinguishable Li signals (Figure S8). As shown in Figure 2d, after sputtering with argon ions the Ca 2p spectra displays two peaks centered at approximately 345.5 and 349.0 eV, which correspond to  $2p_{1/2}$  and  $2p_{3/2}$  energy levels

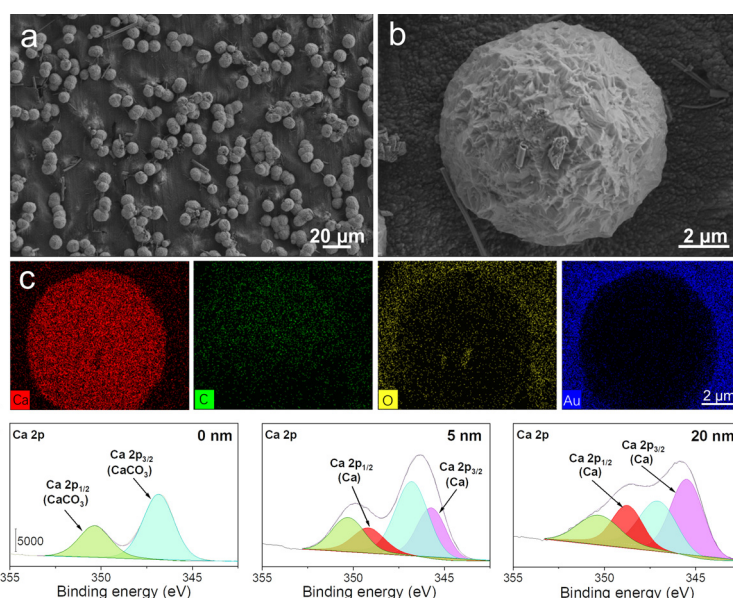


**Figure 2.** a,b) Ca plating morphology in the  $\text{Ca}(\text{BH}_4)_2$ -LiBH<sub>4</sub>-THF electrolyte at 0.25  $\text{mA cm}^{-2}$  and 0.5  $\text{mAh cm}^{-2}$ . c) The elemental distribution of the plating Ca by EDX. d) XPS depth profiling analysis of the deposits in the  $\text{Ca}(\text{BH}_4)_2$ -LiBH<sub>4</sub>-THF electrolyte. The XPS sample was prepared by plating 0.5  $\text{mAh cm}^{-2}$  of deposits on a Au electrode after 3 galvanostatic cycles at 0.25  $\text{mA cm}^{-2}$  and 0.5  $\text{mAh cm}^{-2}$ .

of metallic Ca. From the C 1s spectrum, strong intensities associated with C–C species (ca. 284.8 eV) were observed on the deposited surface in both electrolytes; that is,  $\text{Ca}(\text{BH}_4)_2$ -THF and  $\text{Ca}(\text{BH}_4)_2$ -LiBH<sub>4</sub>-THF (Figure S7), along with the peak centered at about 290.0 eV, which belongs to a C=O species and a weak peak associated with a C–O species at approximately 286.4 eV. All of these species come from THF, since neither  $\text{Ca}(\text{BH}_4)_2$  nor LiBH<sub>4</sub> contain elemental carbon. C–C species derived from THF have not been reported previously,<sup>[4]</sup> which indicates that THF undergoes a different decomposition pathway in this work, but the mechanism requires further investigations. The dominant peak of the O 1s spectrum at about 531.0 eV indicates the presence of C=O species, which agrees with the C 1s spectrum. The Ca 2p peaks centered at 346.9 and 350.4 eV suggest that  $\text{CaCO}_3$  may exist in the passivation layers. Surprisingly, no significant difference was found for the passivation layers formed in these two electrolytes. This suggests that the huge differences in cycling performance probably do not come from compositional differences of the passivation layers.

To investigate the coordination environment of  $\text{Ca}^{2+}$ , the electrolytes were studied using  $^{43}\text{Ca}$  NMR spectroscopy.<sup>[11]</sup> Figure 3a compares the  $^{43}\text{Ca}$  NMR spectra of the  $\text{Ca}(\text{BH}_4)_2$ -LiBH<sub>4</sub>-THF and  $\text{Ca}(\text{BH}_4)_2$ -THF electrolytes. The spectrum of the  $\text{Ca}(\text{BH}_4)_2$ -THF electrolyte shows a narrow peak centered at about 21.4 ppm. At a lower concentration of  $\text{Ca}(\text{BH}_4)_2$  (0.5 M), the chemical shift of the  $^{43}\text{Ca}$  nucleus is about 19.1 ppm (Figure S9). The upfield shift of  $^{43}\text{Ca}$  signals (ca. 2.3 ppm) suggest that additional THF molecules coordinate to Ca and thereby increase the shielding effect on the Ca nucleus. Surprisingly, after introduction of LiBH<sub>4</sub>, a roughly 16.1 ppm downfield shift of  $^{43}\text{Ca}$  (ca. 37.5 ppm) was seen for

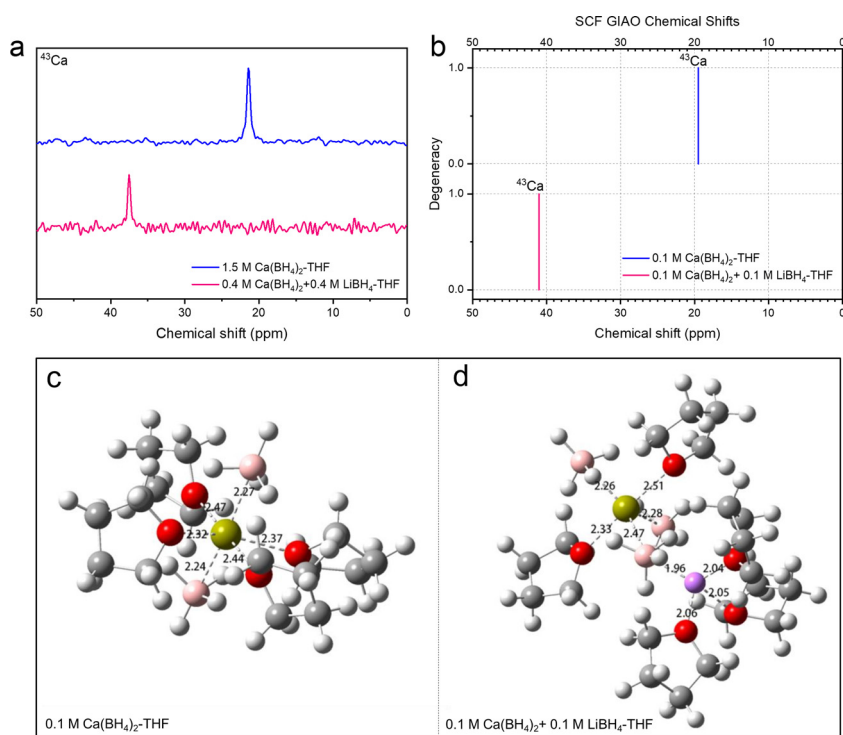


**Figure 3.** a)  $^{43}\text{Ca}$  NMR spectra of two electrolytes. b) The calculated chemical shifts of the pure  $\text{Ca}(\text{BH}_4)_2\text{-THF}$  electrolyte and the  $\text{Ca}(\text{BH}_4)_2\text{-LiBH}_4\text{-THF}$  electrolyte. The local structure of c) pure  $\text{Ca}(\text{BH}_4)_2\text{-THF}$  and d)  $\text{Ca}(\text{BH}_4)_2\text{-LiBH}_4\text{-THF}$  electrolytes. Key: Ca (green), O (red), Li (purple), C (gray), B (pink).

the  $\text{Ca}(\text{BH}_4)_2\text{-LiBH}_4\text{-THF}$  electrolyte, suggesting a much weaker shielding effect on the Ca nucleus.

To deeply understand the solvation structure change of  $\text{Ca}^{2+}$  in the electrolytes,  $^{43}\text{Ca}$  NMR chemical shifts and radial distribution functions were simulated to explain the reduction of shielding effect on the Ca nucleus within the  $\text{Ca}(\text{BH}_4)_2\text{-LiBH}_4\text{-THF}$  electrolyte (for computational details, see the Supporting Information). The calculated results also suggest drastic differences in the chemical shift and coordination environment of the Ca nucleus in two electrolytes (Figures 3b–d; Table S2). The calculated  $^{43}\text{Ca}$  NMR chemical shifts are 19.5 and 41.0 ppm for the pure  $\text{Ca}(\text{BH}_4)_2\text{-THF}$  and  $\text{Ca}(\text{BH}_4)_2\text{-LiBH}_4\text{-THF}$  electrolytes, respectively. Molecular dynamics (MD) simulations suggest that, when  $\text{LiBH}_4$  is added to the  $\text{Ca}(\text{BH}_4)_2\text{-THF}$  electrolyte the local structure of the solute should change and the agglomeration of dual salts may occur. The radial distribution function (Figure S10) reveals that the coordination number of oxygen in the first solvation shell of  $\text{Ca}^{2+}$  is reduced by about 40% in the  $\text{Ca}(\text{BH}_4)_2\text{-LiBH}_4\text{-THF}$  electrolyte, in comparison with that for the pure  $\text{Ca}(\text{BH}_4)_2\text{-THF}$  electrolyte. This lowers the electron density in the first solvation of the  $\text{Ca}^{2+}$  ion, thus weakening the shielding effect on the Ca nucleus and contributing to the corresponding downfield shift of  $^{43}\text{Ca}$  NMR signals upon introduction of  $\text{LiBH}_4$  to the  $\text{Ca}(\text{BH}_4)_2\text{-THF}$  electrolyte. With a lower oxygen density in the first solvation shell of  $\text{Ca}^{2+}$ , the overall solvation energy of  $\text{Ca}^{2+}$  is decreased in the  $\text{Ca}(\text{BH}_4)_2\text{-LiBH}_4\text{-THF}$  electrolyte. Therefore, the desolvation process of  $\text{Ca}^{2+}$  at the electrode/

electrolyte interface should be more kinetically favorable, which is consistent with CV scans and the overpotential of the Ca-plating/stripping processes. Since the desolvation process is considered as the rate-determining step for electroplating,<sup>[12]</sup> better kinetics for this process are helpful for Ca plating/stripping.

The high reversibility of Ca plating and stripping in the  $\text{Ca}(\text{BH}_4)_2\text{-LiBH}_4\text{-THF}$  electrolyte allowed us to build up a real CMB using Ca metal as an anode material. The  $\text{Ca}(\text{BH}_4)_2\text{-LiBH}_4\text{-THF}$  electrolyte was used in a  $\text{Ca}||$  lithium titanate (LTO) cell to verify its feasibility and stability in a full cell configuration. In this cell, the Ca-metal anode undergoes stripping and plating processes upon cycling, while the LTO cathode takes the intercalation chemistry for  $\text{Li}^+$ . As shown in Figure 4a, the  $\text{Ca}||$  LTO cell delivers a first discharge specific capacity of about  $170 \text{ mAh g}^{-1}$ . Remarkably, the full cell demonstrates 200 stable discharge/charge cycles with a capacity retention of roughly 80% (Figure 4b). The stable cycling performance of the  $\text{Ca}||$  LTO battery indicates an excellent stability of the Ca-metal anode in the  $\text{Ca}(\text{BH}_4)_2\text{-LiBH}_4\text{-THF}$  electrolyte. In contrast, the  $\text{Ca}||$  LTO battery cycled with the  $\text{Ca}(\text{BH}_4)_2\text{-THF}$  electrolyte shows a very limited specific capacity (ca.  $25 \text{ mAh g}^{-1}$ ), suggesting its incompatibility with the full cell configuration (Figure S11).

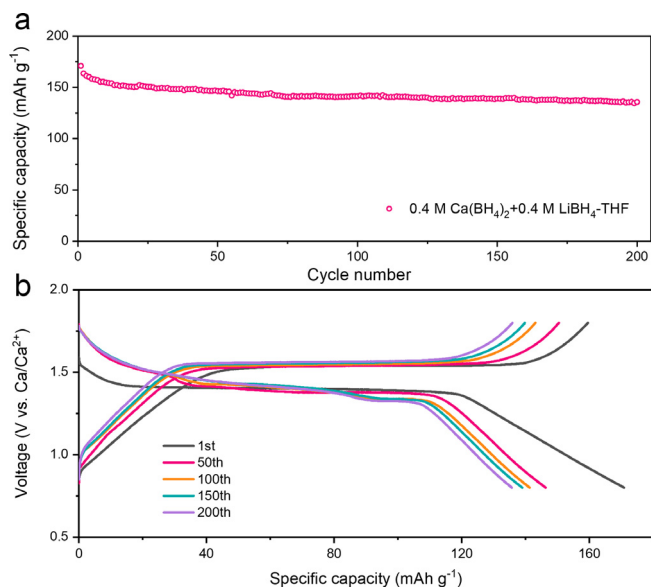


**Figure 4.** a) The discharge specific capacity of LTO cathode material in a  $\text{Ca}||$  LTO full cell with the  $\text{Ca}(\text{BH}_4)_2\text{-LiBH}_4\text{-THF}$  electrolyte under galvanostatic cycling at 0.2 C ( $1 \text{ C} = 175 \text{ mAh g}^{-1}$ ). b) Voltage–capacity profile of the  $\text{Ca}||$  LTO full cell at selected cycles.

In summary, we report a facile and effective strategy for significantly improving the reversibility of a Ca-metal anode. By manipulating the solvation structure of Ca ions, the room-temperature reversible plating and stripping of Ca metal is realized. The addition of LiBH<sub>4</sub> salt dramatically decreases the coordination number of Ca<sup>2+</sup> in the first solvation shell, thus lowering the solvation energy of the electrolyte. Galvanostatic Ca-plating/stripping processes are highly reversible in the Ca(BH<sub>4</sub>)<sub>2</sub>-LiBH<sub>4</sub>-THF electrolyte, with a record-high CE up to 99.1% and a very stable and long lifespan over 200 cycles. The Ca||LTO full cell delivers high capacity retention (ca. 80%) after 200 cycles, which demonstrates the viability of the Ca(BH<sub>4</sub>)<sub>2</sub>-LiBH<sub>4</sub>-THF electrolyte for practical applications. This work offers a promising strategy to design optimized nonaqueous electrolytes for Ca-metal batteries.

### Acknowledgements

This work was supported by the National Key Research and Development Program of China (Grant No. 2017YFA0402802 and 2017YFA0206700), the National Natural Science Foundation of China (Grant No. 51902304 and 21776265), Anhui Provincial Natural Science Foundation (Grant No. 1908085ME122), and the Fundamental Research Funds for the Central Universities (Wk2060140026).

### Conflict of interest

The authors declare no conflict of interest.

**Keywords:** calcium plating · Coulombic efficiency · cycle life · solvation structure

- [1] a) D. Aurbach, Z. Lu, A. Schechter, Y. Gofer, H. Gizbar, R. Turgeman, Y. Cohen, M. Moshkovich, E. Levi, *Nature* **2000**, 407, 724; b) P. Canepa, G. Sai Gautam, D. C. Hannah, R. Malik, M. Liu, K. G. Gallagher, K. A. Persson, G. Ceder, *Chem. Rev.* **2017**, 117, 4287–4341; c) J. Muldoon, C. B. Bucur, T. Gregory, *Chem. Rev.* **2014**, 114, 11683–11720; d) M.-C. Lin, M. Gong, B. Lu, Y. Wu, D.-Y. Wang, M. Guan, M. Angell, C. Chen, J. Yang, B.-J. Hwang, H. Dai, *Nature* **2015**, 520, 324; e) J. Muldoon, C. B. Bucur, T. Gregory, *Angew. Chem. Int. Ed.* **2017**, 56, 12064–12084; *Angew. Chem.* **2017**, 129, 12232–12253; f) J. Muldoon, C. B. Bucur, A. G. Oliver, T. Sugimoto, M. Matsui, H. S. Kim, G. D. Allred, J. Zajicek, Y. Kotani, *Energy Environ. Sci.* **2012**, 5, 5941–5950.
- [2] a) M. E. Arroyo-de Dompablo, A. Ponrouch, P. Johansson, M. R. Palacín, *Chem. Rev.* **2020**, <https://doi.org/10.1021/acs.chemrev.9b00339>; b) T. Ouchi, H. Kim, B. L. Spatocco, D. R. Sadoway, *Nat. Commun.* **2016**, 7, 10999; c) R. J. Gummow, G. Vamvounis, M. B. Kannan, Y. He, *Adv. Mater.* **2018**, 30, 1801702.
- [3] a) S.-B. Son, T. Gao, S. P. Harvey, K. X. Steirer, A. Stokes, A. Norman, C. Wang, A. Cresce, K. Xu, C. Ban, *Nat. Chem.* **2018**, 10, 532; b) R. Mohtadi, M. Matsui, T. S. Arthur, S. J. Hwang, *Angew. Chem. Int. Ed.* **2012**, 51, 9780–9783; *Angew. Chem.* **2012**, 124, 9918–9921; c) X. Sun, P. Bonnicksen, V. Duffort, M. Liu, Z. Rong, K. A. Persson, G. Ceder, L. F. Nazar, *Energy Environ. Sci.* **2016**, 9, 2273–2277; d) M. Walter, K. V. Kravchik, M. Ibanez, M. V. Kovalenko, *Chem. Mater.* **2015**, 27, 7452–7458.
- [4] D. Wang, X. Gao, Y. Chen, L. Jin, C. Kuss, P. G. Bruce, *Nat. Mater.* **2018**, 17, 16.
- [5] a) D. Aurbach, R. Skaletsky, Y. Gofer, *J. Electrochem. Soc.* **1991**, 138, 3536–3545; b) A. Ponrouch, M. Palacín, *Curr. Opin. Electrochem.* **2018**, 9, 1–7.
- [6] S.-Y. Ha, Y.-W. Lee, S. W. Woo, B. Koo, J.-S. Kim, J. Cho, K. T. Lee, N.-S. Choi, *ACS Appl. Mater. Interfaces* **2014**, 6, 4063–4073.
- [7] A. Ponrouch, C. Frontera, F. Bardé, M. R. Palacín, *Nat. Mater.* **2016**, 15, 169.
- [8] a) Z. Li, O. Fuhr, M. Fichtner, Z. Zhao-Karger, *Energy Environ. Sci.* **2019**, 12, 3496–3501; b) A. Shyamsunder, L. E. Blanc, A. Assoud, L. F. Nazar, *ACS Energy Lett.* **2019**, 4, 2271–2276.
- [9] a) M. Wang, C. Jiang, S. Zhang, X. Song, Y. Tang, H.-M. Cheng, *Nat. Chem.* **2018**, 10, 667; b) S. Wu, F. Zhang, Y. Tang, *Adv. Sci.* **2018**, 5, 1701082; c) Z. Yao, V. I. Hegde, A. Aspuru-Guzik, C. Wolverton, *Adv. Energy Mater.* **2019**, 9, 1802994.
- [10] a) Y. Shao, T. Liu, G. Li, M. Gu, Z. Nie, M. Engelhard, J. Xiao, D. Lv, C. Wang, J.-G. Zhang, J. Liu, *Sci. Rep.* **2013**, 3, 3130; b) T. Liu, J. T. Cox, D. Hu, X. Deng, J. Hu, M. Y. Hu, J. Xiao, Y. Shao, K. Tang, J. Liu, *Chem. Commun.* **2015**, 51, 2312–2315; c) J. Luo, S. He, T. L. Liu, *ACS Energy Lett.* **2017**, 2, 1197–1202; d) X. Chen, H.-R. Li, X. Shen, Q. Zhang, *Angew. Chem. Int. Ed.* **2018**, 57, 16643–16647; *Angew. Chem.* **2018**, 130, 16885–16889; e) X. Q. Zhang, X. Chen, X. B. Cheng, B. Q. Li, X. Shen, C. Yan, J. Q. Huang, Q. Zhang, *Angew. Chem. Int. Ed.* **2018**, 57, 5301–5305; *Angew. Chem.* **2018**, 130, 5399–5403; f) X.-Q. Zhang, X. Chen, L.-P. Hou, B.-Q. Li, X.-B. Cheng, J.-Q. Huang, Q. Zhang, *ACS Energy Lett.* **2019**, 4, 411–416.
- [11] R. M. Farmer, A. I. Popov, *Inorg. Nucl. Chem. Lett.* **1981**, 17, 51–56.
- [12] K. Xu, *J. Electrochem. Soc.* **2007**, 154, A162–A167.

Manuscript received: February 13, 2020

Revised manuscript received: March 17, 2020

Accepted manuscript online: April 8, 2020

Version of record online: May 25, 2020